Electronic Supplementary Material (ESI) for Journal of Materials Chemistry C.

Supporting Information

Halogen Doping of p-type Inorganic Hole Transport Layer: Electronic Nature Based Dopant Engineering for Modulating Hole Selectivity in Inverted Planar Perovskite Solar Cells

*Vidya Sudhakaran Menon[a], Saraswathi Ganesan[a], Rohith Kumar Raman[b], Ananthan Alagumalai[a], Ananthanarayanan Krishnamoorthy[a]**

[a]Organic and Perovskite Photovoltaics Laboratory (OPPV), Department of Chemistry, SRM Institute of Science and Technology, Kattankulathur, Tamil Nadu, India, Pin Code-603203.

[b]Department of Physics and Nanotechnology, SRM Institute of Science and Technology, Kattankulathur, Tamil Nadu, India, Pin Code-603203.

E-mail: ananthak@srmist.edu.in

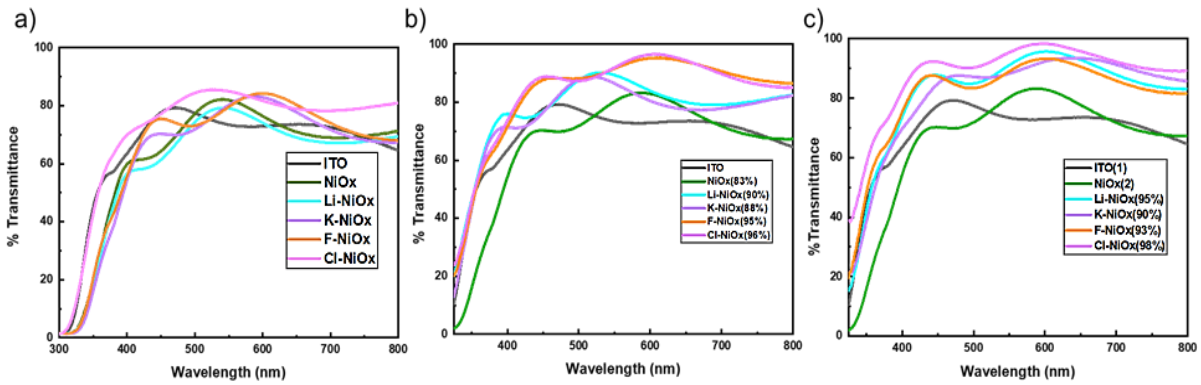

Figure S1. % Transmittance plots of a) 10 wt. % doped b) 3 wt. % doped and c) 1 wt. % doped NiO_x thin films.

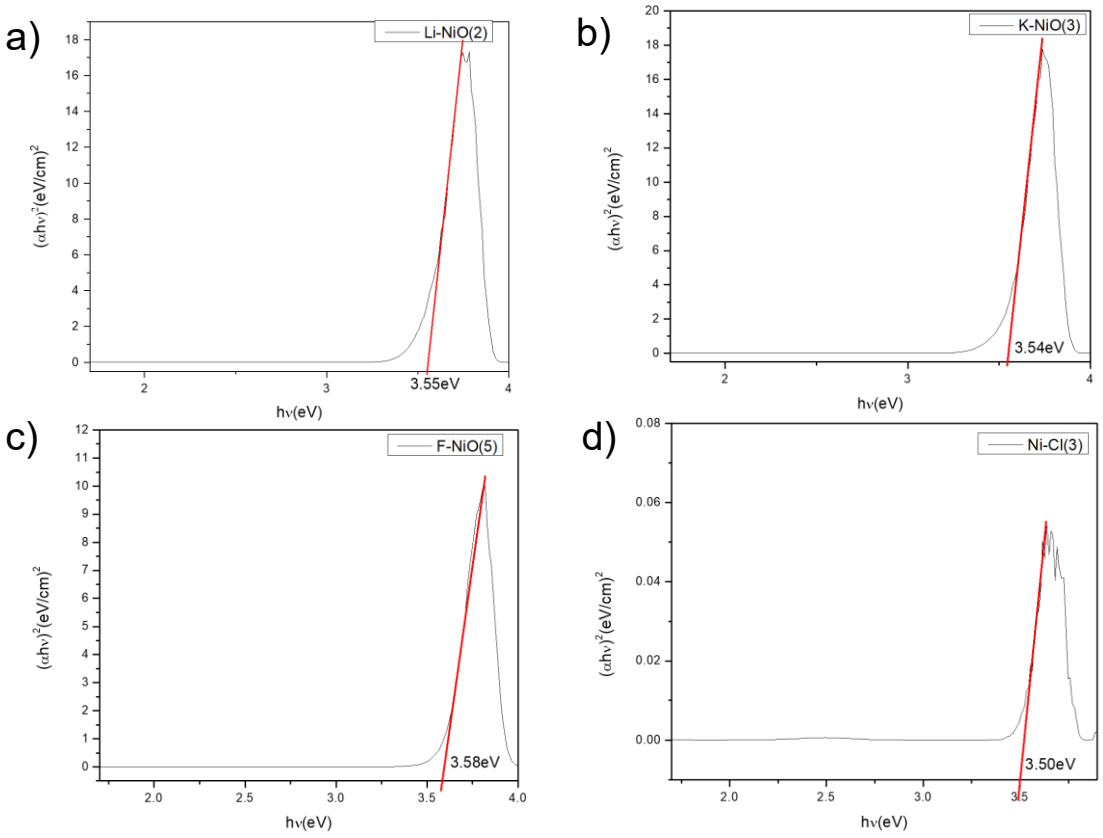

Figure S2. Tauc plot of 10 wt. % doped a) Li:NiO_x b) K:NiO_x c) F:NiO_x and d) Cl:NiO_x.

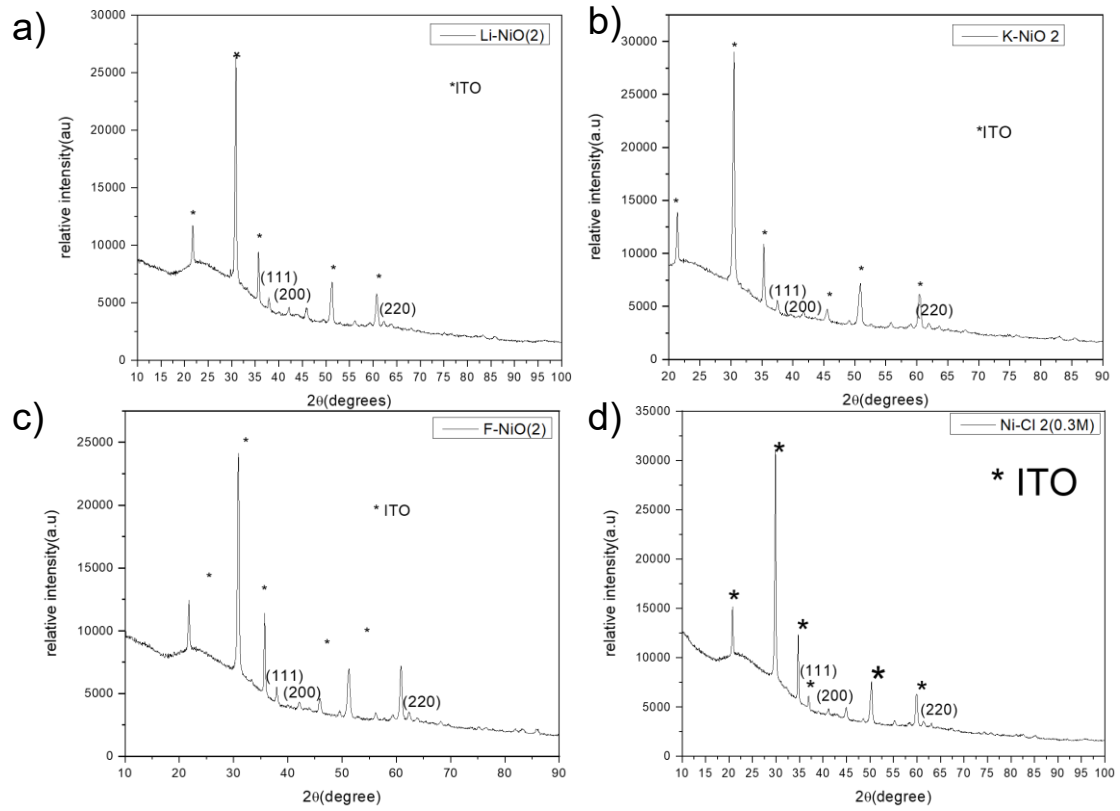

Figure S3. XRD plot of 10 wt. % doped a) Li:NiO_x b) K:NiO_x c) F:NiO_x and d) Cl:NiO_x.

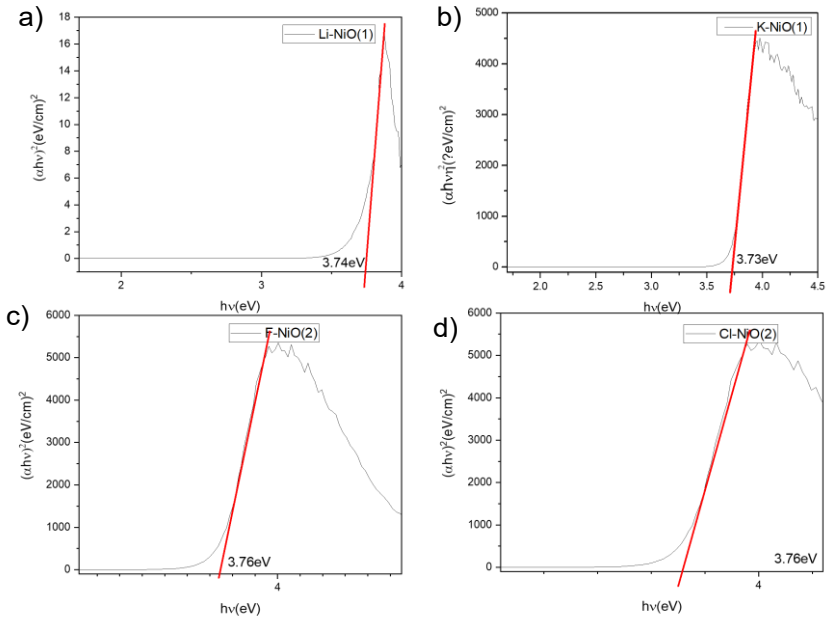

Figure S4. Tauc plot of 3 wt. % doped a) Li:NiO_x b) K:NiO_x c) F:NiO_x and d) Cl:NiO_x.

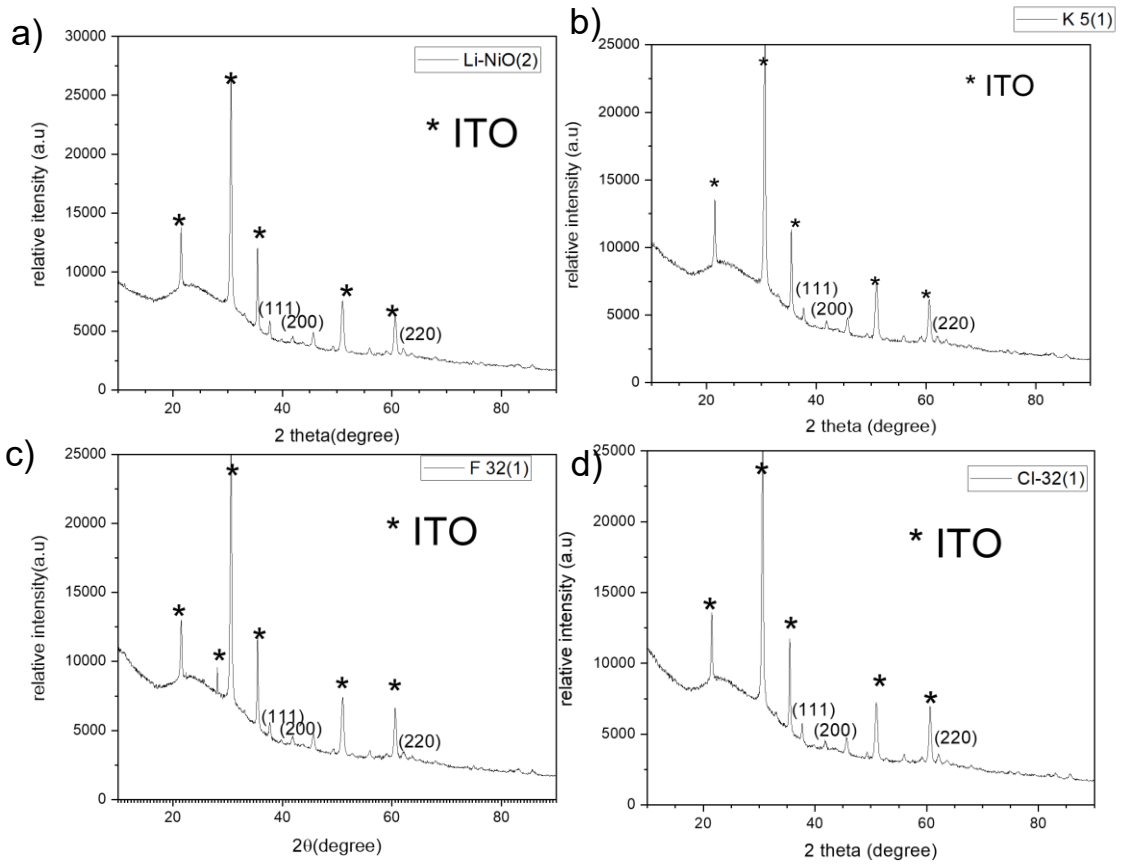

Figure S5. XRD plot of 3 wt. % doped a) Li:NiO_x b) K:NiO_x c) F:NiO_x and d) Cl:NiO_x.

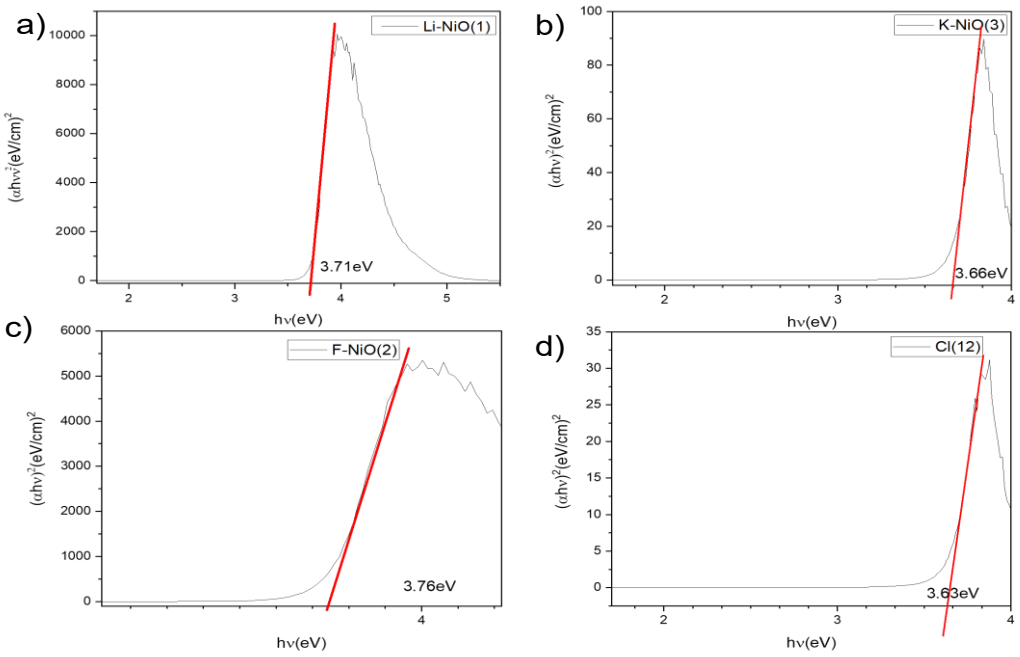

Figure S6. Tauc plot of 1 wt. % doped a) Li:NiO_x b) K:NiO_x c) F:NiO_x and d) Cl:NiO_x.

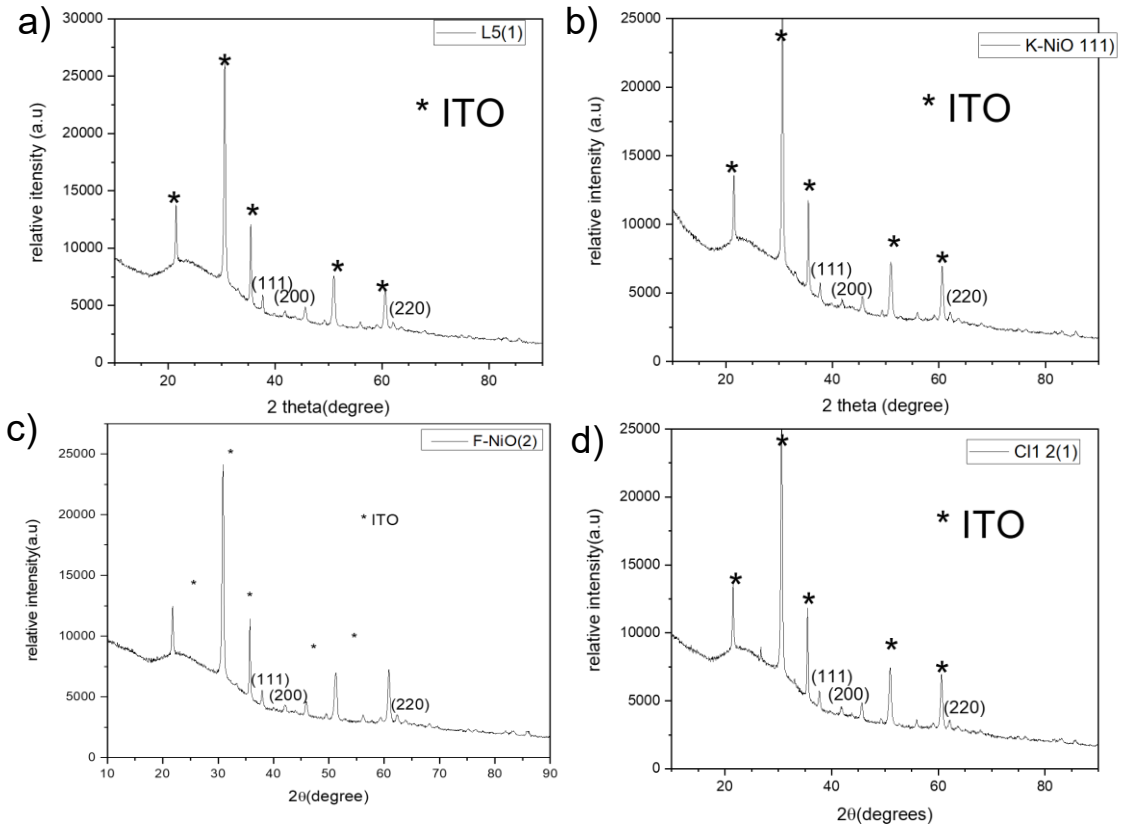

Figure S7. XRD plot of 1 wt. % doped a) Li:NiO_x b) K:NiO_x c) F:NiO_x and d) Cl:NiO_x.

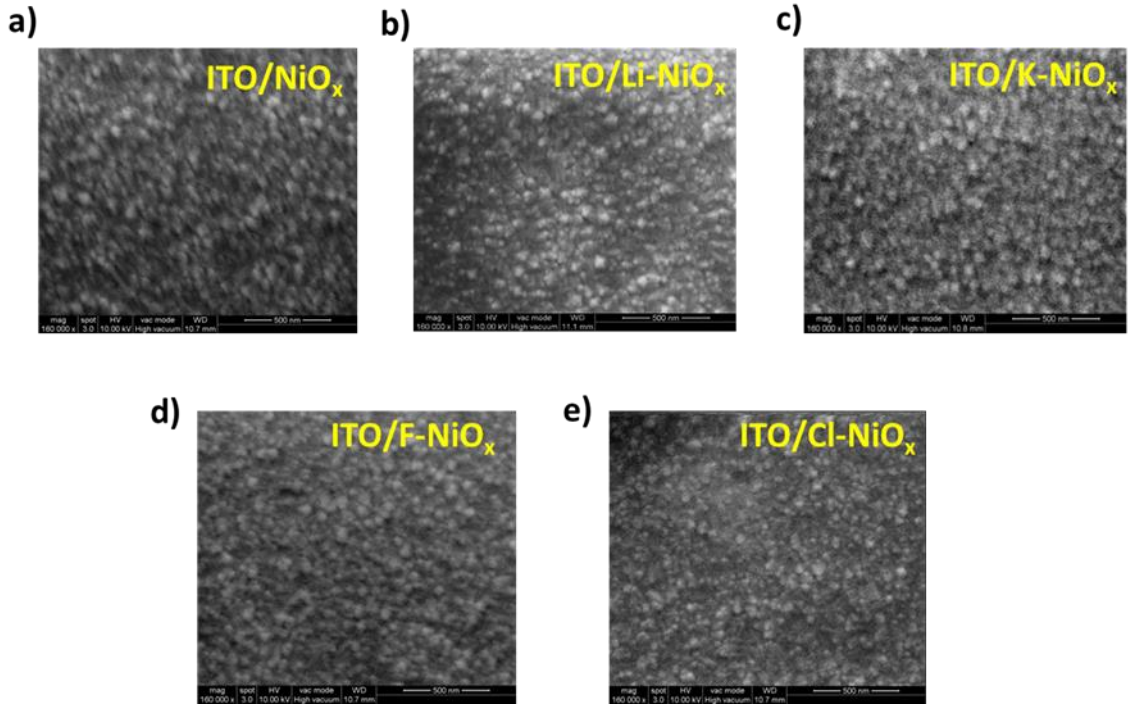

Fig.S8. SEM images of a) undoped NiO_x b) Li:NiO_x c) K:NiO_x d) F:NiO_x and e) Cl:NiO_x

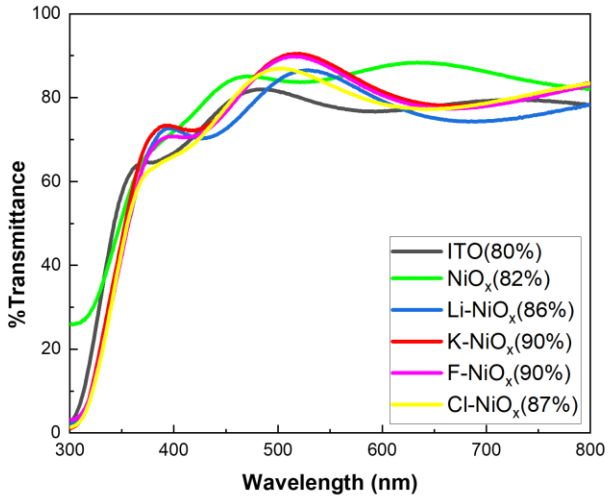

Figure S9. % Transmittance plots of undoped and 5 wt. % doped NiO_x thin films.

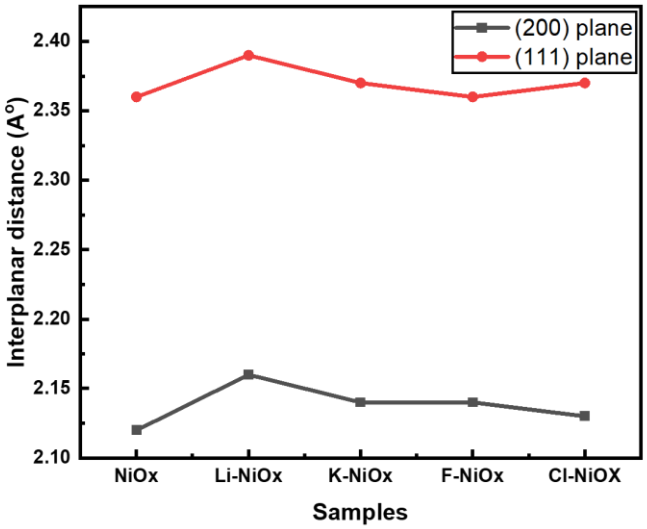

Fig. S10. Plot of interplanar spacing in undoped and 5 wt. % doped NiO_x

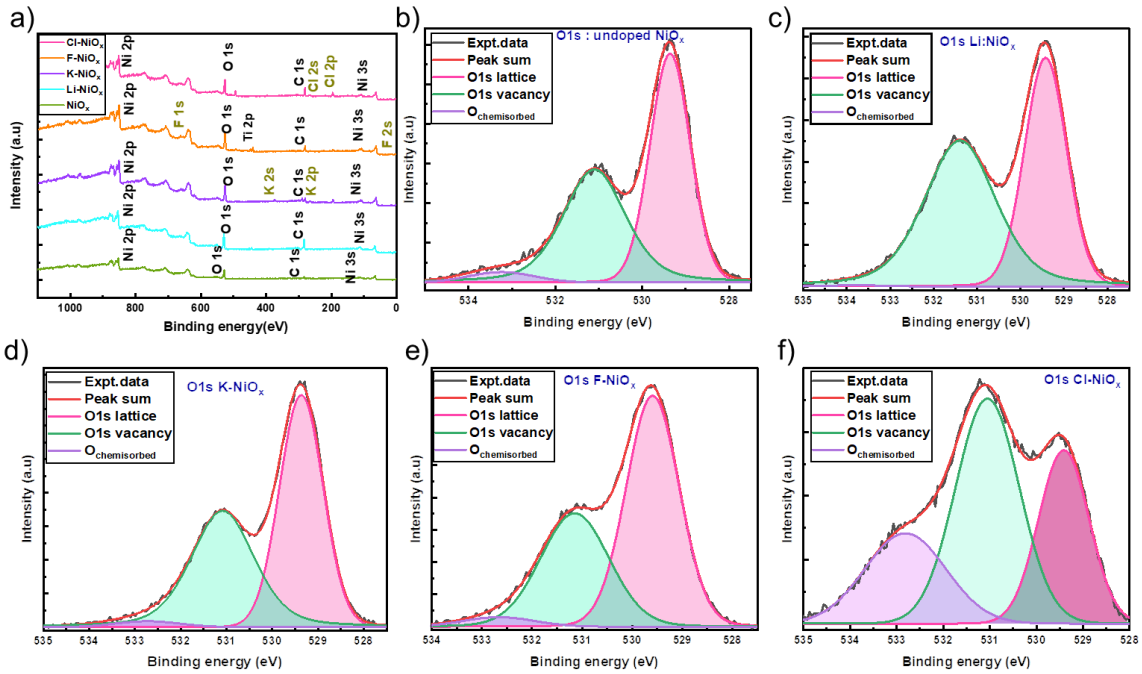

Fig. S11. a) XPS survey scan for undoped and doped NiO_x samples. O1s deconvoluted spectra for b) NiO_x c) $Li:NiO_x$ d) $K:NiO_x$ e) $F:NiO_x$ and f) $Cl:NiO_x$.

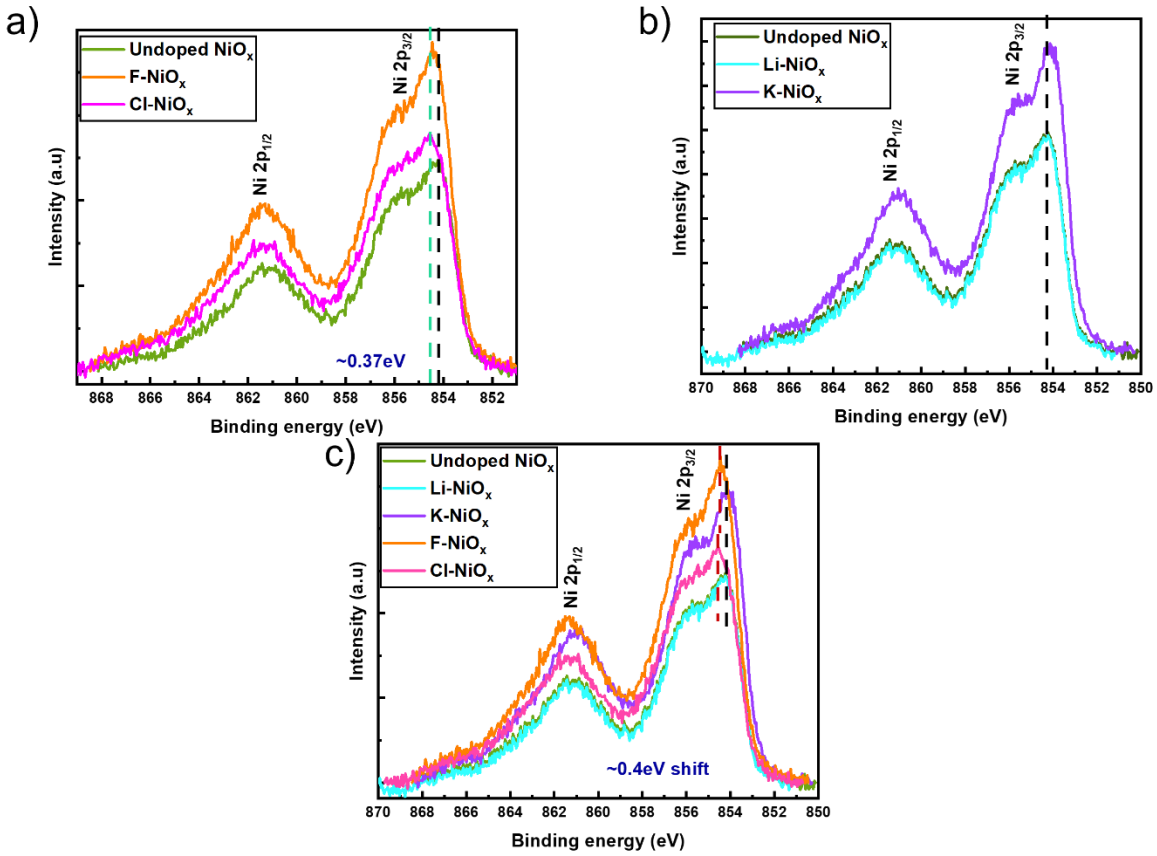

Fig. S12. Peak shift analysis of a) undoped NiO_x and F and Cl-doped NiO_x thin films b) undoped NiO_x and Li and K-doped NiO_x thin films and c) Correlative analysis of peak shift in undoped and doped NiO_x thin films.

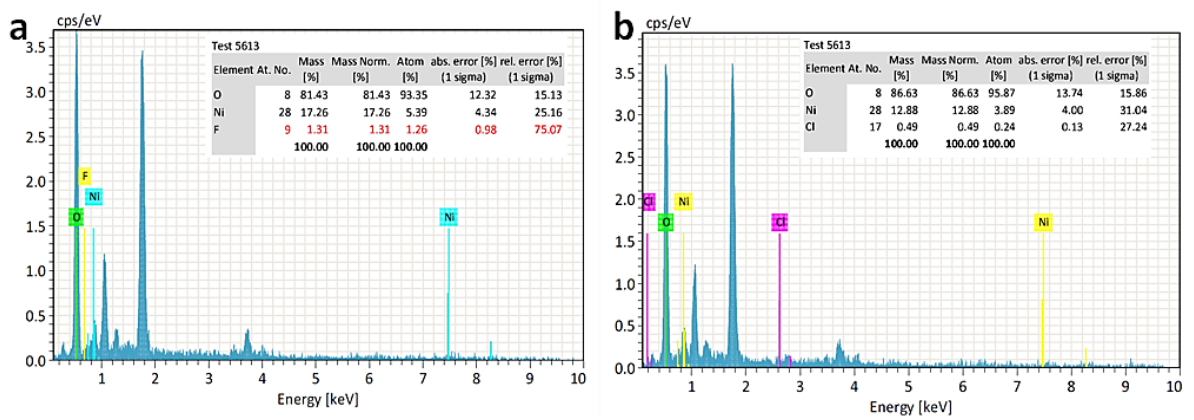

Fig. S13. EDS spectra of a) F:NiO_x and b) Cl:NiO_x

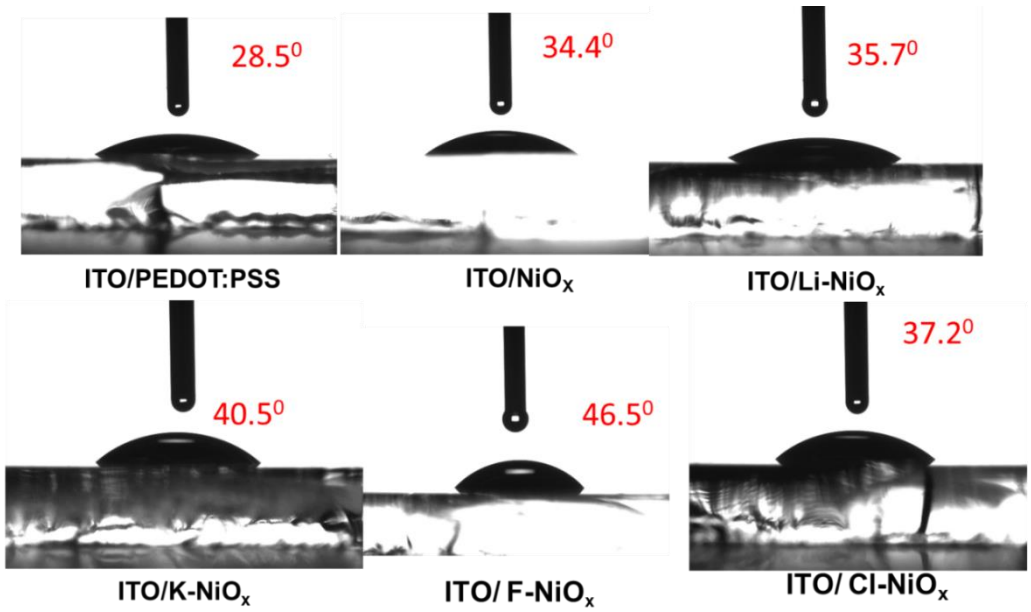

Fig. S14. Water contact angle on PEDOT:PSS, doped and undoped NiO_x thin films.

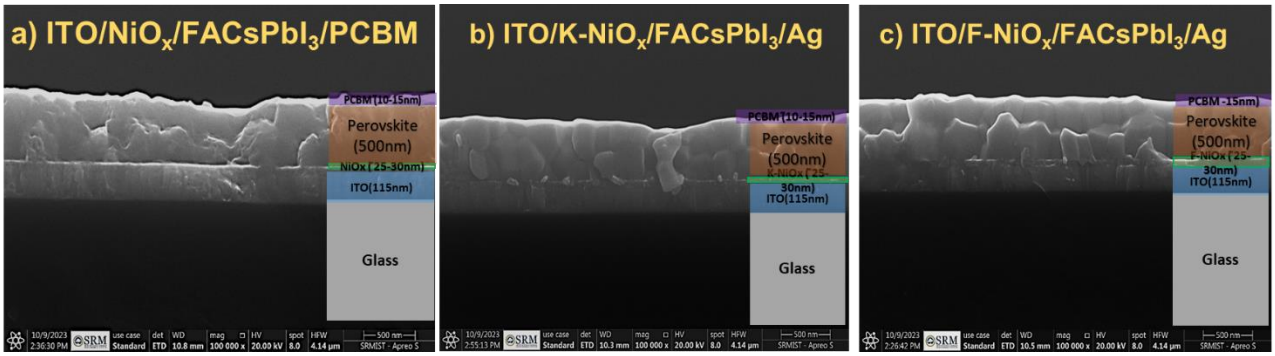

Fig. S15. Cross-section images of $FACsPbI_3$ absorber on a) NiO_x b) $K:NiO_x$ and c) $F:NiO_x$.

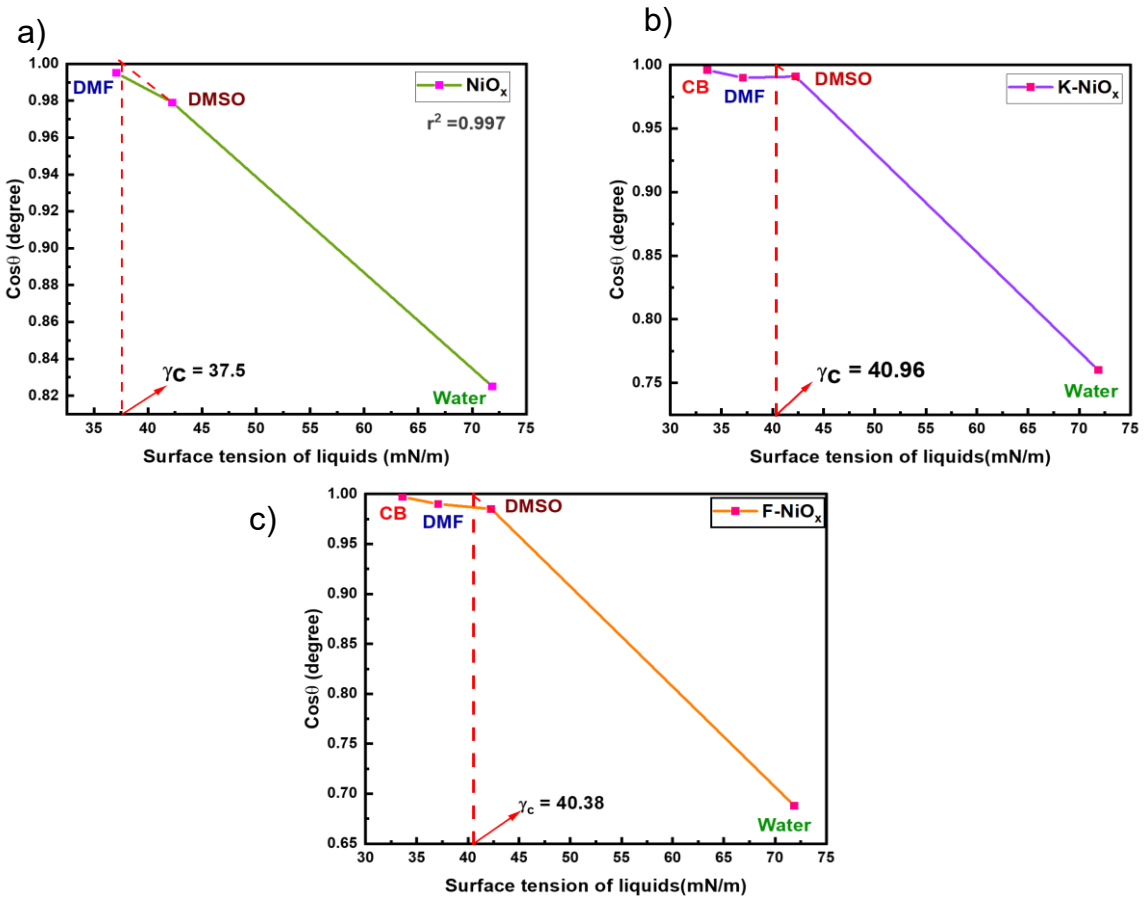

Fig. S16. Zisman plot of a) NiO_x b) $K:NiO_x$ and c) $F:NiO_x$.

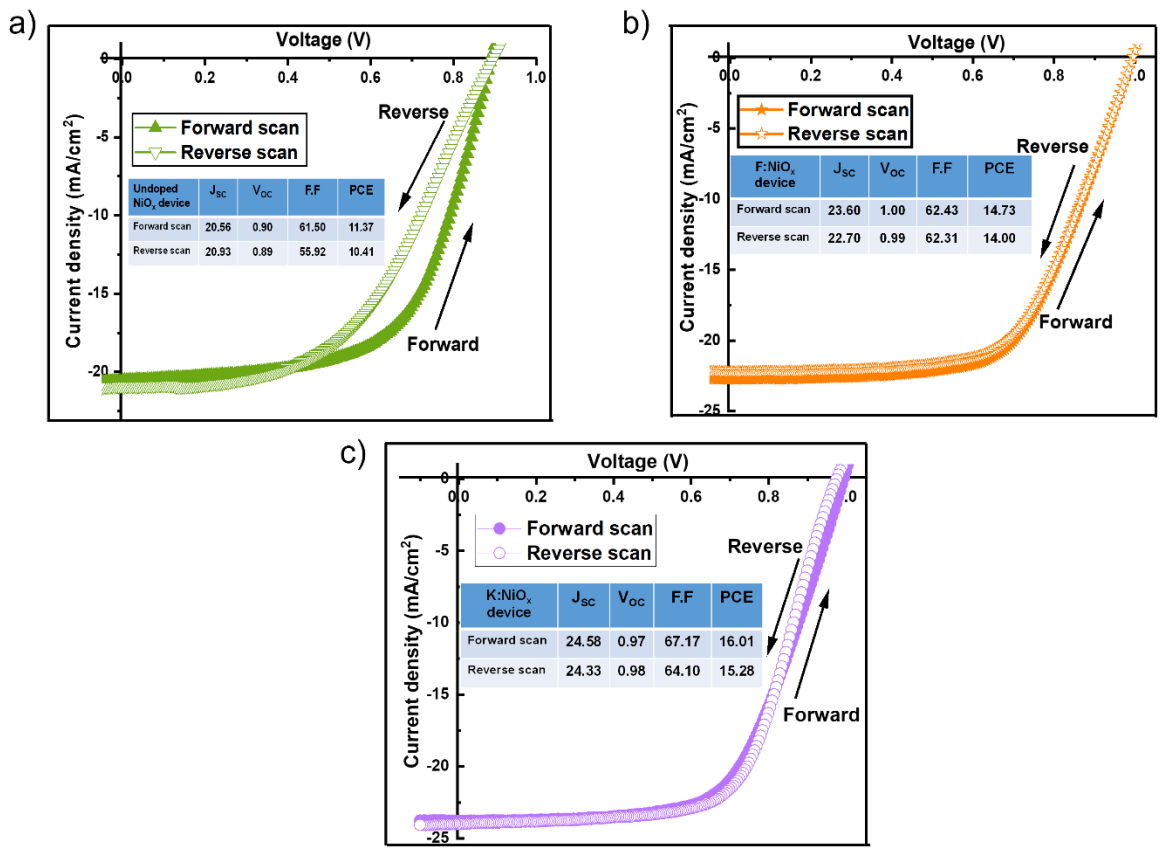

Fig. S17. Forward and reverse scan of J-V data for a) undoped NiO_x b) F:NiO_x and c) K:NiO_x devices. A Keithley 2400 source meter was used for the current-voltage scan by applying an external voltage bias and measuring the response current with a scan rate of 120 mV s^{-1} under reverse and forward scan conditions. The devices were not subjected to any preconditioning techniques before to the measurement, such as applying a forward voltage bias or performing extended light soaking.

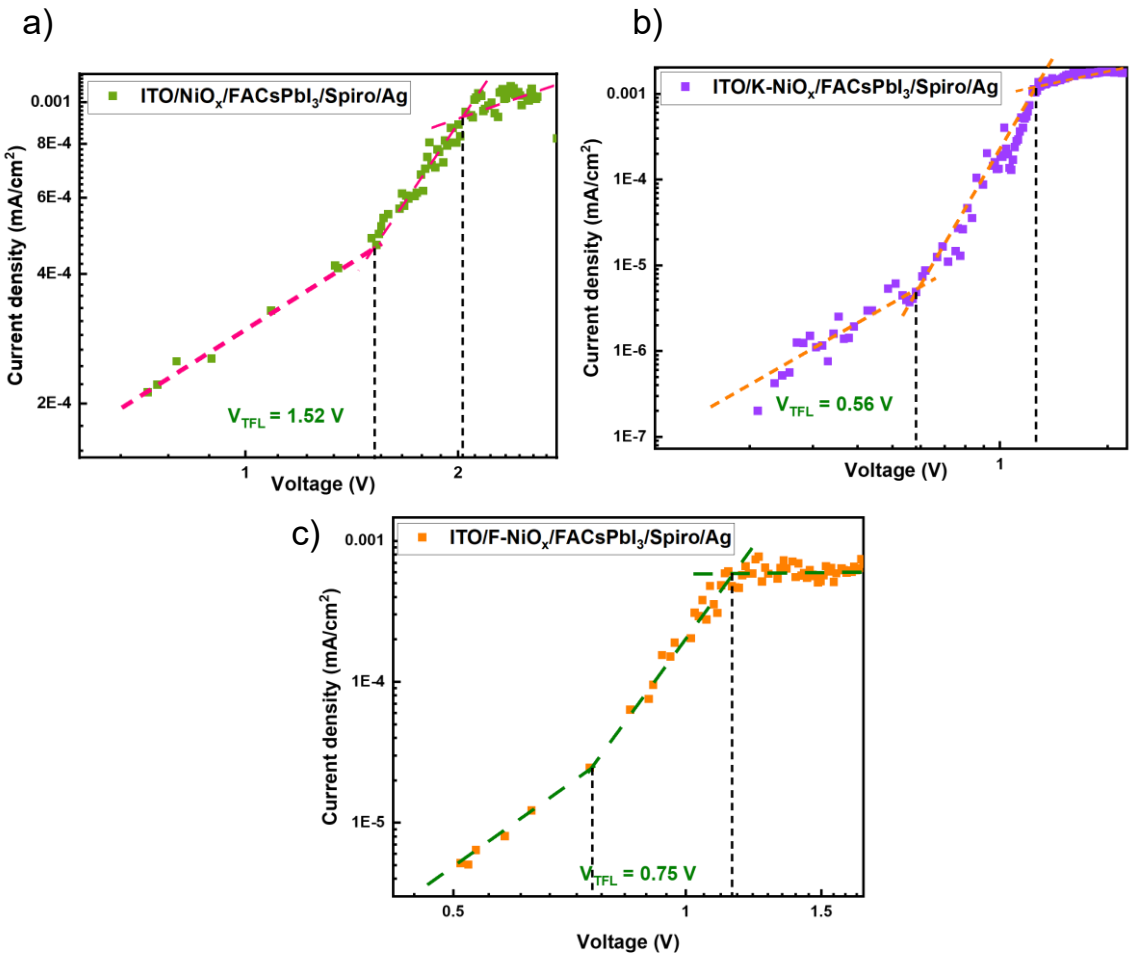

Fig. S18. SCLC plot for a) undoped NiO_x b) K-doped NiO_x and c) F-doped NiO_x based hole only devices

Table S1. % WAT values of doped and undoped NiO_x thin films

Sample	% WAT
ITO	83.85 %
NiO_x	74.30 %
Li:NiO_x	77.31 %
K:NiO_x	75.34 %
F:NiO_x	80.07 %
Cl:NiO_x	75.13 %

Table S2. Peak fitting parameters for

a) **Undoped NiO_x**

Peak	Peak position	FWHM	Peak area	χ^2	Ni^{3+}/Ni^{2+} ratio
Ni^{2+}	854.13	1.36	10016.20	1.54	0.90
Ni^{3+} shoulder peak	855.86	3.0	9045.54		
Ni^{2+} satellite peak	861.02	3.23	10839.41		
Ni^{3+} satellite peak	863.37	4.28	3502.31		

b) Li:NiO_x

Peak	Peak position	FWHM	Peak area	χ^2	Ni^{3+}/Ni^{2+} ratio
Ni^{2+}	853.95	1.33	6226.81	1.29	3.10
Ni^{3+} shoulder peak	855.64	3.05	19352.34		
Ni^{2+} satellite peak	860.91	3.90	14767.49		
Ni^{3+} satellite peak	864.26	4.59	3069.81		

c) K:NiO_x

Peak	Peak position	FWHM	Peak area	χ^2	Ni^{3+}/Ni^{2+} ratio	Wt. % of dopant found in sample
Ni^{2+}	853.93	1.28	2414.32	1.38	3.27	1.56
Ni^{3+} shoulder peak	855.64	3.18	7826.21			
Ni^{2+} satellite peak	860.91	3.80	4967.95			
Ni^{3+} satellite peak	864.26	6.21	3132.94			

d) F:NiO_x

Peak	Peak position	FWHM	Peak area	χ^2	Ni^{3+}/Ni^{2+} ratio	Wt. % of dopant found in sample
Ni^{2+}	854.22	1.31	5686.78	1.13	3.83	0.41
Ni^{3+} shoulder peak	855.78	3.24	19849.70			
Ni^{2+} satellite peak	861.19	4.08	20038.58			
Ni^{3+} satellite peak	864.32	4.86	3121.85			

e) Cl:NiO_x

Peak	Peak position	FWHM	Peak area	χ^2	Ni^{3+}/Ni^{2+} ratio	Wt. % of dopant found in sample
Ni^{2+}	854.23	1.42	4249.77	1.24	3.49	2.07
Ni^{3+} shoulder peak	855.86	3.32	16315.03			
Ni^{2+} satellite peak	861.14	3.88	10670.18			
Ni^{3+} satellite peak	863.34	6.36	5542.51			

Table S3. Crystallite size of $FA_{0.9}Cs_{0.1}PbI_3$ absorber on doped and undoped NiO_x HTL.

Thin film sample	Interplanar spacing (Å)	Crystallite size (nm)
1) Undoped NiO_x/$FACsPbI_3$	6.15	62.2
2) K-NiO_x/$FACsPbI_3$	6.17	87.7
3) F-NiO_x/$FACsPbI_3$	6.20	109.1

Table S4. Surface energy values of doped and undoped NiO_x HTL.

Thin film sample	Surface energy (mJ/m^2)
1) Undoped NiO_x	37.50
2) Li:NiO_x	38.74
3) K:NiO_x	40.96
4) F:NiO_x	40.38
5) Cl:NiO_x	40.90